CrossMark
click for updates

Achieving rough sphere-shaped ZnS with superior attenuation electromagnetic absorption performance

Yan-chun Sun,†[a] Dong-ping Li,†[b] Ying Yang,†[b] Li-shuang Fan,[c] Song Wu,[a] Peng Wang*[a] and Yi Song*[d]

ZnS micrometer spheres were prepared *via* a facile hydrothermal route. Polyvinyl pyrrolidone (PVP) was used as the surfactant. By controlling the PVP content, the smooth surface of ZnS sphere was converted to a rough surface, which led to a stronger electromagnetic wave scattering intensity when used as an electromagnetic absorption absorber. ZnS microspheres with the roughest surface showed the best electromagnetic absorption property. The absorption frequency of this product at 2.0 mm was 4.2 GHz. The minimum reflection loss was nearly −35.0 dB, indicating excellent attenuation ability. The attenuation mechanism is discussed in detail and was attributed to the scattering effect.

1. Introduction

Recently, the application of an electromagnetic absorber to treat the increasing electromagnetic wave interference (EMI) has attracted considerable attention.[1,2] This functional material can make the electromagnetic wave incident on the absorption layer and convert it to thermal energy, depending on its intrinsic attenuation ability.[3] To achieve a good electromagnetic absorption performance, better impedance matching behavior is the key to ensure less reflection of electromagnetic wave from the interface of the absorption layer. The incoming electromagnetic wave can then be attenuated because of the intrinsic physic loss features. Currently, metal oxides have are the desired absorbers owing to the impedance matching and attenuation ability.[4,5] Currently, representative metal oxides, such as Fe_3O_4,[6] $CoFe_2O_4$,[7] NiO,[8] and CuO,[9] have been widely applied in electromagnetic absorption studies. For example, the optimal reflection loss of CoO nanoparticles prepared by Li *et al.* was estimated to be −37.0 dB.[10] The minimum reflection loss (RL_{min}) for the $Co_xFe_{3-x}O_4$ was up to −41.089 dB at a thickness of 2.0 mm, according to the Ji's report.[11] The binary $NiCo_2O_4$/

CoNiO$_2$ sample also showed a RL_{min} value less than −40 dB with a thickness of 1.5 mm.[12] Compared to metal oxides, recent research has shown that metal sulfides presented better dielectric loss ability if used in the electromagnetic absorber field.[12,13] The primary reason is the improved conductive ability.[14] According to the electromagnetic absorption mechanism, the improved conductive ability can lead to an increase in permittivity. In this case, the dielectric loss ability of metal sulfides is prominently stronger than those of the corresponding metal oxides notwithstanding a slight decrease in impedance matching performance.[15] For example, Lv and co-workers developed the $Fe_{0.5}Ni_{0.5}Co_2S_4$ composite and obtained a RL_{min} value of −14.0 dB with a thin coating thickness of 1.5 mm. At the same time, the frequency region of RL <−10 dB was nearly 6.2 GHz.[16] Through a simple top-down exfoliation method, few-layer MoS_2 was achieved, the RL_{min} value was approximately −38.42 dB and the frequency bandwidth was 4.1 GHz with a thickness of 2.4 mm.[17] In addition, the Fe_3S_4 introduced by Liu *et al.* had a minimum reflection loss of −36.03 dB with a thickness of 3.0 mm.[18]

Owing to the advantages of easy production and low-cost, considerable efforts have been focused on the ZnS absorber.[19] In addition to these merits, ZnS also presents moderate conductive behavior and results in impedance matching and dielectric loss ability. Therefore, the development of ZnS is considered to be another efficient strategy to gain the desired electromagnetic absorber. In this study, sphere-like ZnS was obtained using a simple hydrothermal strategy. By controlling the contents of the surfactant, the ZnS surface was becoming increasingly rough. The electromagnetic absorption properties of these ZnS spheres were studied.

[a]Heilongjiang River Fisheries Research Institute of Chinese Academy of Fishery Sciences, Laboratory of Quality & Safety Risk Assessment for Aquatic Products (Harbin), Ministry of Agriculture, Harbin 150070, P. R. China. E-mail: Wapg911@126.com; Tel: +86-0451-84861321

[b]College of Chemical and Environmental Engineering, Harbin University of Science & Technology, Harbin 150080, P. R. China

[c]Academy of Fundamental and Interdisciplinary Sciences, Harbin Institute of Technology, Harbin 150080, P. R. China

[d]Chinese Academy of Fishery Sciences, Beijing 100141, P. R. China. E-mail: songyi@cafs.ac.cn; Fax: +86-0451-84604803

† These authors contributed equally to this work.

2. Experiment

2.1 Synthesis of ZnS sphere

Sphere-like ZnS was prepared *via* a facile hydrothermal process. Typically, 0.1 g zinc acetate (Zn(Ac)$_2$) and 0.5 g thiourea (TA) were dispersed in 60 mL of distilled water (DI) for 30 min ultrasonic treatment to form a clear solution. A certain amount of pyrrolidone polyvinyl (PVP) was dispersed into the above-mentioned solution to serve as the surfactant. After another 10 min of ultrasonic treatment, the abovementioned solution was transferred to a 100 mL autoclave and heated at 150 °C for 12 hours. After natural cooling, the precipitate was collected *via* centrifugation and washed several times with ethanol and distilled water. Finally, sphere-like ZnS was achieved after drying the precipitate at 60 °C for one day. The ZnS spheres obtained with the addition of 0, 10, 20, and 30 mg of PVP are denoted as ZS-1, ZS-2, ZS-3 and ZS-4, respectively.

2.2 Measurement

X-ray diffraction (XRD, Rigaku Desktop X-ray diffractometer, Cu Kα radiation) was employed to test the crystalline phase of the ZnS samples: (test region: 20–70°, wavenumber $\lambda = 0.15418$ nm; scanning voltage = 40 keV). The morphology of the samples was observed *via* Field Emission Scanning Electron Microscopy (FE-SEM, JEOL JSM-7100F) and equipped with Electron Energy Disperse Spectroscopy (EDS). The X-ray photoelectron spectrum was obtained on a PHI 5000 VersaProbe systems, in which an Al Kα X-ray source was operated at 150 W. At the same time, a TEM image was obtained on a Tecnai G220 S-Twin. The complex permittivity and permeability parameters were measured on an Agilent 8722ES network analyzer. The cylindrical sample (inner diameter of 3.04 mm and outer diameter of 7.0 mm) was fabricated by uniformly mixing a paraffin matrix with 60 wt% absorbents, and the composite was then pressed into a cylindrical mold. Transmission line theory was used to calculate the reflection loss.

3. Results and discussion

The morphology of ZnS sample (ZS-1) was characterized by FE-SEM. A sphere-structure can be observed in Fig. 1a. These ZnS spheres without adding PVP presented a smooth surface (in Fig. 2b). According to Fig. 1c, this ZnS sphere has a solid structure. Through EDS, only Zn and S signals were detected and the corresponding atomic ratio of Zn/S was 52.1 to 48.9, which is approximately 50 : 50 (seen Fig. 1e). Fig. 1f also showed that the diameters of these ZnS spheres were primarily distributed in the range 5–7 μm. In addition, a small part of the ZnS spheres was smaller than 1.0 μm, indicating that the size of these ZnS sphere is not uniform. Fig. 1f presents the XRD pattern of the sample. These diffraction peaks were matched to the standard XRD card (JCPDS card no: 75-1534) without other impurity peaks. X-ray photoelectron spectroscopy (XPS) revealed the binding energy values of Zn at 1022 and 1045 eV, which were attributed to $2p_{3/2}$ and $2p_{1/2}$ of Zn^{2+}. At the same time, the binding energy of S 2p was 162 eV, corresponding to S^{2-}.[20]

In this study, the initial content of PVP plays a key role in the final structure. Fig. 3a–c show the ZnS obtained with a mass of 10, 20 and 30 mg. Through the FE-SEM images, the ZnS with varying content of PVP still showed a spherical structure. However, the surface of the ZnS spheres became more rugged with increasing PVP content.

The electromagnetic absorption properties of these ZnS samples were tested using a coaxial-line method. The electromagnetic parameters, including real/imaginary part of permittivity ($\varepsilon'/\varepsilon''$) as well as the permeability (μ'/μ'') were also obtained. The reflection loss at 2–18 GHz was calculated using the following equations:[21,22]

$$Z_{in} = Z_o(\mu_r/\varepsilon_r)^{1/2} \tanh[j(2\pi fd(\mu_r\varepsilon_r)^{1/2}/c)] \tag{1}$$

$$RL\ (dB) = 20\log|(Z_{in} - Z_o)/(Z_{in} + Z_o)| \tag{2}$$

$$\mu_r = \mu' - j\mu'' \tag{3}$$

$$\varepsilon_r = \varepsilon' - j\varepsilon'' \tag{4}$$

where Z_{in} is the input impedance of the absorber; Z_o accounts for the characteristic impedance of free space (377 Ω); f is the frequency of electromagnetic wave; d is the coating thickness of the absorber; c is the velocity of the light and μ_r and ε_r are the complex permeability and permittivity values. For a desired electromagnetic absorber, the minimum reflection loss should be less than −10 dB (corresponding to 90% of absorption and attenuation). The frequency region of RL <−10 dB is better when it is as broad as possible (denoted as the qualified frequency region). The reflection loss *vs.* frequency curves are given in Fig. 4. The qualified frequency bandwidth of ZS-1 was approximately 2.0 GHz (14–16 GHz) with a coating thickness of 2.0 mm. At other thicknesses ($d = 2.5$ or 3.0 mm), the qualified frequency bandwidth was smaller than 2.0 GHz and the corresponding minimum reflection loss was larger than −15.0 dB. For ZS-2, however, the qualified frequency bandwidth was narrow and not more than 1.0 GHz at 2.0 mm, indicating a poor microwave absorption ability. For other thicknesses, the reflection loss of ZS-2 was even larger than −10 dB, as shown in Fig. 4b. In Fig. 4c, the qualified frequency bandwidth for ZS-3 was estimated to be 3.8 GHz (14.2–18 GHz) at 2.0 mm. In addition, the optimal reflection loss increased in the range from −15 to −20 dB. Further enhancement was observed for the ZS-4 sample, in which the frequency bandwidth at 2.0 mm was larger than 4.0 GHz (13.8–18 GHz). The electromagnetic absorption properties of ZS-4 are better than those of the similar products, as listed in Table 1.[23–28] Most importantly, the RL$_{min}$ value at 2.5 mm was below −35 dB, which was highest of these samples. Therefore, it can be concluded that ZS-4 achieved the strongest electromagnetic absorption ability while that of ZS-2 was poor.

To analyze the electromagnetic attenuation mechanism, the real and imaginary parts of permittivity are listed in Fig. 5a and b (for the nonmagnetic material, the real part of permeability was a constant value of 1.0 and the imaginary part of the permeability value was almost 0).[29] Based on the
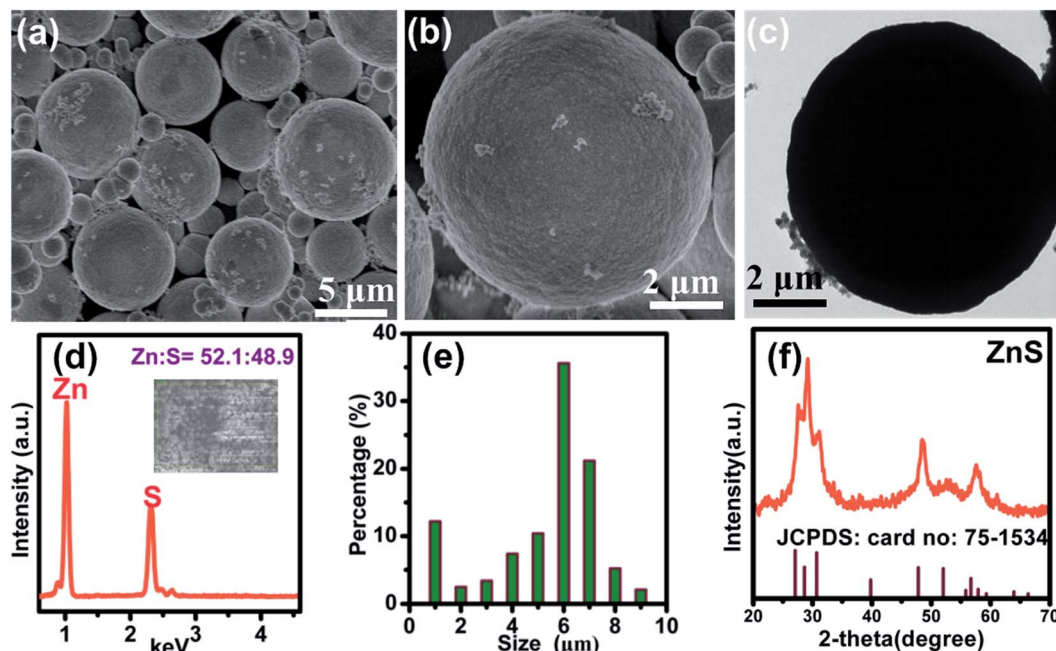
Fig. 1 (a and b) FE-SEM images (c) the TEM image of the ZnS prepared without PVP; (d) EDS spectrum (e) and size distribution of these ZnS micrometer spheres without the addition of PVP. (f) XRD patterns of the ZnS without PVP.
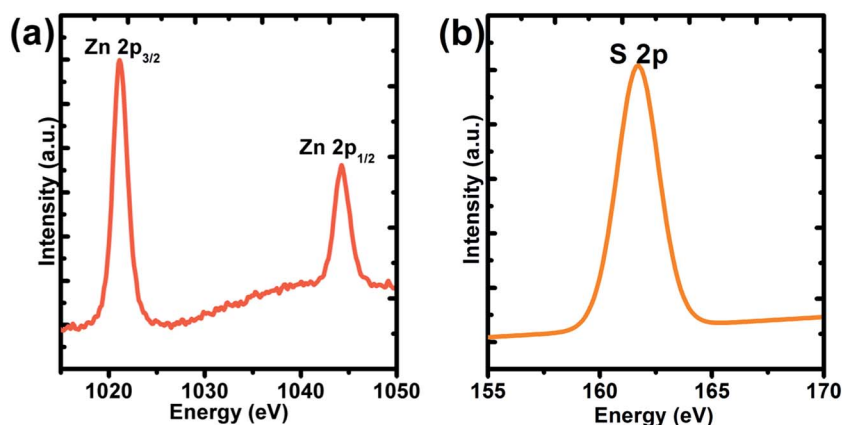

Fig. 2 XPS spectrum of the ZnS spheres prepared without the addition of PVP. (a) Zn 2p; (b) S 2p.
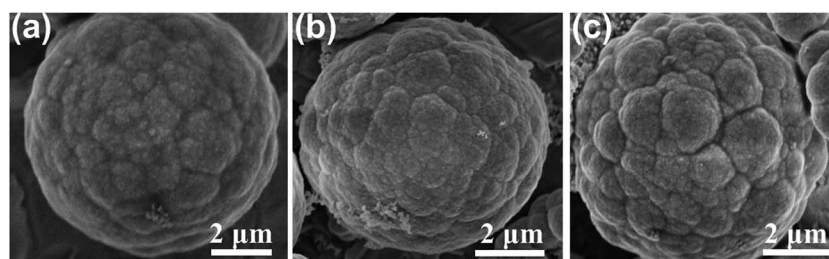

Fig. 3 FE-SEM images of the ZnS spheres with various amounts of PVP: (a) 10 mg; (b) 20 mg; (c) 30 mg.

electromagnetic absorption mechanism, the role of impedance matching and attenuation (including the dielectric and magnetic loss ability) is to determine the final electromagnetic absorption ability. In Fig. 4a, these ε' values follow the order ZS-1 < ZS-2 < ZS-3 < ZS-4. Generally, a larger ε' value indicates the better storage electrical ability but damages to the impedance
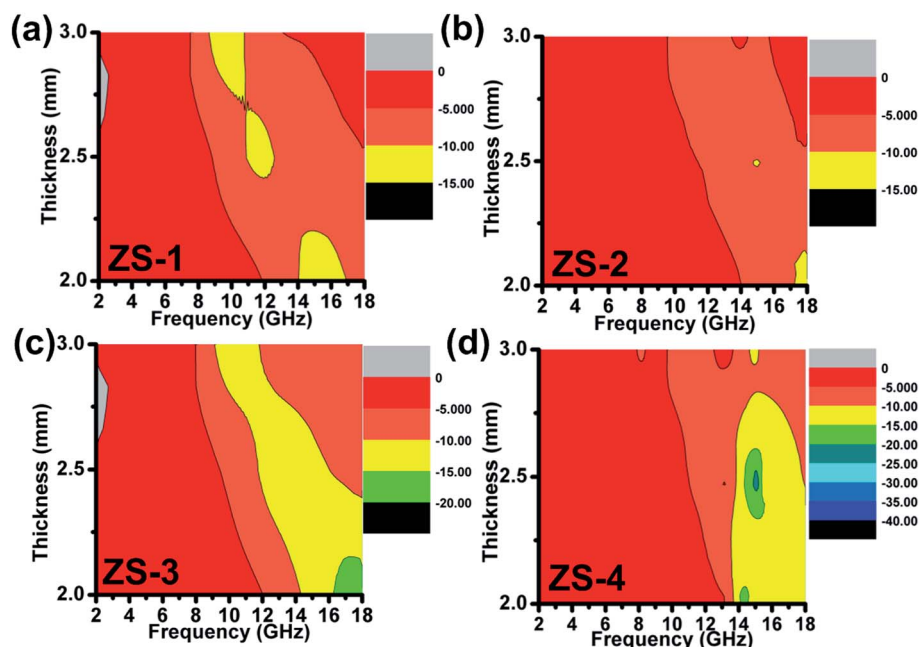
Fig. 4 Electromagnetic absorption spectrum of the ZnS samples: (a) ZS-1; (b) ZS-2; (c) ZS-3; (d) ZS-4.

Table 1 Electromagnetic absorption properties of similar metal sulfides

Sample	f_E (GHz)	RL_{min} (dB)	Filled ratio (wt%)	Thickness (mm)	Ref.
ZnS	<2.0	−11.02	70	2.5	23
CuS	~3.0	−25.0	10	2.0	24
CoS	0.0	<−10.0	40	2.0	25
MoS_2	0.0	<−10.0	10	2.0	26
MnS	0.0	<−10.0	40	3.0	27
CuS/ZnS	0 GHz	<−10 dB	N.A	2.0	28
ZnS	4.2 GHz	−18 dB	60	2.0	In this work

matching performance.[30] The ε'' value refers to the dielectric loss ability. For these nonmagnetic ZnS samples, the attenuation ability resulted was only from the dielectric loss. As shown

in Fig. 5b, ZS-4 showed the largest ε'' value (1.8–2.0), whereas ZS-1 showed the smallest value over the entire frequency region (1.2–0.8). Several peaks could be observed at a higher frequency region for the ZS-1, ZS-2 and ZS-3 products. Generally, these peaks could be assigned to the dipolar polarization effect.[31,32] The ε'' value cannot fully stand for the attenuation ability. If one absorber has a smaller ε' value, the larger ε'' value does not contribute to the final dielectric loss ability. Therefore, the effective attenuation ability generally can be calculated based on the following equation:[33,34]

$$\alpha = \frac{\sqrt{2}\pi f}{c} \times \sqrt{(\mu''\varepsilon'' - \mu'\varepsilon') + \sqrt{(\mu''\varepsilon'' - \mu'\varepsilon')^2 + (\mu'\varepsilon'' + \mu''\varepsilon')^2}}$$

(5)

where α is the effective attenuation constant. A bigger α value generally indicates stronger effective attenuation ability. Among

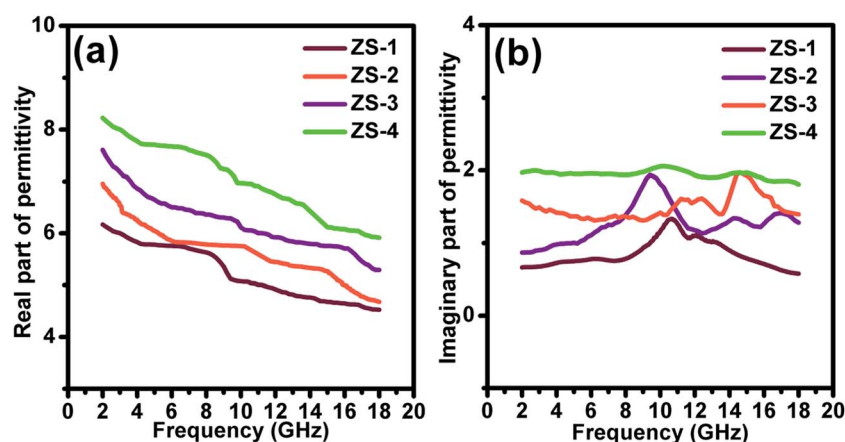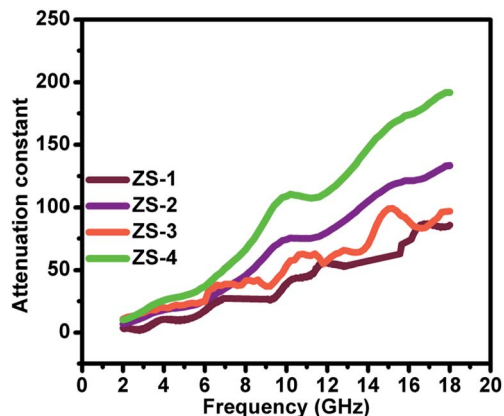**Fig. 5** Real (a) and imaginary (b) part of permittivity ZnS samples.

Fig. 6 Attenuation constant of the ZnS samples.

these samples, ZS-4 presented the largest α value, whereas ZS-1 showed the smallest, as indicated in Fig. 6. For the electromagnetic absorption properties, the ZS-1 sample was better than ZS-2, which could be explained by the improved impedance matching behavior (Fig. 7).

The dielectric loss is composed mainly of the conductive and polarization forms. Generally, conductive loss occurs in a highly conductive material, which should be ruled out for these ZnS materials.[35] Considering the polarization effect, it generally involves the relaxation process, which can be expressed by the Cole–Cole semicircle. The relative complex permittivity can be described by the following equation:[36,37]

$$\varepsilon_r = \varepsilon_\infty + \frac{\varepsilon_s - \varepsilon_\infty}{1 + j2\pi f \tau} = \varepsilon' - j\varepsilon'' \qquad (6)$$

where ε_s, ε_∞, and τ are static permittivity, relative dielectric permittivity at high-frequency limit, and polarization relaxation time, respectively. Therefore, ε' and ε'' can be calculated using the following equations.

$$\varepsilon' = \varepsilon_\infty + \frac{\varepsilon_s - \varepsilon_\infty}{1 + (2\pi f)^2 \tau^2} \qquad (7)$$

$$\varepsilon'' = \frac{2\pi f \tau (\varepsilon_s - \varepsilon_\infty)}{1 + (2\pi f)^2 \tau^2} \qquad (8)$$

Based on eqn (7) and (8), the $\varepsilon' - \varepsilon''$ can be expressed as

$$(\varepsilon' - \varepsilon_\infty)^2 + (\varepsilon'')^2 = (\varepsilon_s - \varepsilon_\infty)^2 \qquad (9)$$

Therefore, a plot of $\varepsilon' - \varepsilon''$ should be a semicircle, which is generally called the Cole–Cole semicircle. Each Cole–Cole semicircle indicates one Debye relaxation process. The Debye relaxation process is related to the polarization forms, such as an electron, atomic, dipolar as well interface polarization. On the other hand, these samples do not present the Cole–Cole semicircle, indicating a weak polarization effect. This result is not consistent with the ε'' curve, as mentioned above. In other words, dipolar polarization is not stronger, and hence the Cole–Cole curve could be reflected.
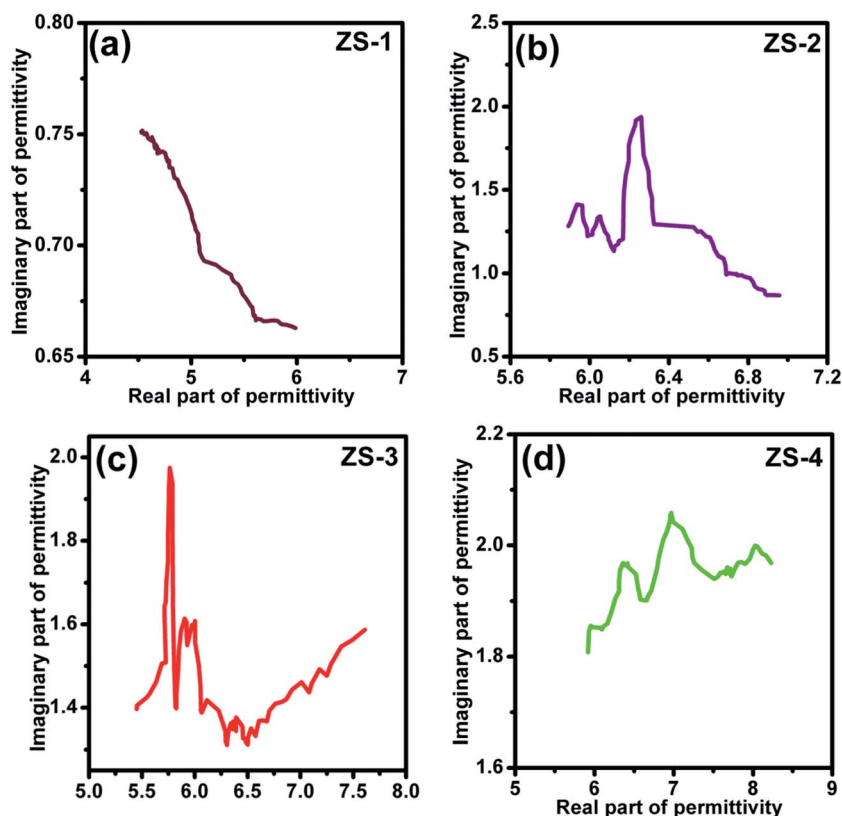
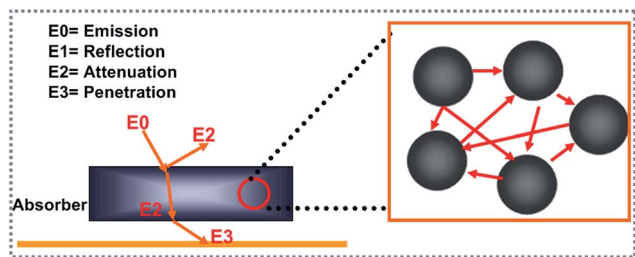

Fig. 7 Cole–Cole curves of the ZnS samples.

Fig. 8 Illustration of the scattering effect mechanism.

The electromagnetic wave scattering effect plays an important role in the attenuation of an electromagnetic wave. The detailed attenuation mechanism can be understood easily from Fig. 8. Generally, the incident electromagnetic wave (E0) can be divided into the following parts. One part of the electromagnetic wave will reflect directly from the absorber interface (E1). Subsequently, the entered electromagnetic wave can be attenuated (E2) or transmitted (E3) to the absorber. Commonly, a stronger scattering intensity results in a decrease in E3. According to the literature, a larger sized (generally larger than a micron) polyhedron structure as well as a rough surface influences the scattering intensity.[38] In this study, the ZS-4 sample with the roughest surface showed the best electromagnetic absorption performance, which may be caused by the stronger scattering effect.

4. Conclusion

Through a simple hydrothermal process, rough spherical ZnS was achieved. Interestingly, the surface of ZnS sphere could be roughened by adding PVP as a surfactant. An analysis of the electromagnetic absorption properties showed that spherical ZnS with the roughest surface presented the stronger dielectric loss ability and electromagnetic absorption properties. In detail, the qualified absorption frequency of the optimal sample at 2.0 mm was up to 4.2 GHz. At the same time, the reflection loss was also less than −30 dB. A study of the attenuation mechanism suggested that these results were due to an electromagnetic scattering effect.

Acknowledgements

References

1 Y. Zhang, Y. Huang, T. F. Zhang, H. C. Chang, P. S. Xiao, H. H. Chen, Z. Y. Huang and Y. S. Chen, *Adv. Mater.*, 2015, **27**, 2049–2053.

2 X. F. Zhang, Y. X. Li, R. G. Liu, Y. Rao, H. W. Rong and G. W. Qin, *ACS Appl. Mater. Interfaces*, 2016, **8**, 3494–3498.

3 H. L. Lv, H. Q. Zhang and G. B. Ji, *Part. Part. Syst. Charact.*, 2016, **33**, 656–663.

4 L. Saini, Y. Janu, M. K. Patra, R. K. Jani, G. K. Gupta and S. R. Vadera, *J. Am. Ceram. Soc.*, 2016, **99**, 3002–3007.

5 M. Zhou, F. Lu, B. T. Liu, J. Yang and X. H. Zeng, *J. Phys. D: Appl. Phys.*, 2015, **48**, 495303–495311.

6 H. L. Lv, G. B. Ji, W. Liu, H. Q. Zhang and Y. W. Du, *J. Mater. Chem. C*, 2015, **3**, 10232–10241.

7 D. Moitra, M. Chandel, B. K. Ghosh, R. Jani, M. K. Patra, S. Vaderab and N. N. Ghosh, *RSC. Adv.*, 2016, **6**, 76759–76772.

8 T. Liu, Y. Pang, X. B. Xie, W. Qi, Y. Wu, S. Kobayashi, J. Zheng and X. G. Li, *J. Alloys Compd.*, 2016, **667**, 287–296.

9 Y. Z. Wan, T. Cui, J. Xiao, G. Y. Xiong, R. S. Guo and H. L. Luo, *J. Alloys Compd.*, 2016, **687**, 334–341.

10 Y. Li, J. Zhang, Z. W. Liu, M. M. Liu, H. J. Lin and R. C. Che, *J. Mater. Chem. C*, 2014, **2**, 5216–5222.

11 R. L. Ji, C. B. Cao, Z. Chen, H. Z. Zhai and J. Bai, *J. Mater. Chem. C*, 2014, **2**, 5944–5953.

12 H. J. Wu, G. L. Wu, Y. Y. Ren, L. Yang, L. D. Wang and X. H. Li, *J. Mater. Chem. C*, 2015, **3**, 7677–7690.

13 J. C. Park and Y. S. Nam, *J. Colloid Interface Sci.*, 2015, **460**, 177–180.

14 X. J. Xu, L. F. Hu, N. Gao, S. X. Liu, S. Wageh, A. Ghamdi, A. Alshahire and X. S. Feng, *Adv. Funct. Mater.*, 2015, **21**, 445–454.

15 X. Z. Lin, A. Ennaoui, S. Levcenko, T. Dittrich, J. Kavalakkatt and S. Kretzschmar, *Appl. Phys. Lett.*, 2015, **106**, 013903–013907.

16 H. L. Lv, H. Q. Zhang, B. S. Zhang, G. B. Ji, Y. He and Q. Lin, *J. Mater. Chem. C*, 2016, **4**, 5476–5482.

17 M. Q. Ning, M. M. Lu, J. B. Li, Z. Chen, Y. K. Dou, C. Z. Wang, F. Rehman, M. S. Cao and H. B. Jin, *Nanoscale*, 2015, **7**, 15734–15740.

18 X. G. Liu, C. Feng, N. N. Bi, Y. P. Sun, J. C. Fan, Y. H. Lv, C. G. Jin, Y. R. Wang and C. T. Li, *Ceram. Int.*, 2014, **40**, 9917–9922.

19 Y. H. Zhang, N. Zhang, Z. R. Tang and Y. J. Xu, *ACS Nano*, 2012, **6**, 9777–9789.

20 J. Y. Park, S. J. Park, J. H. Lee, C. H. Hwang, K. J. Hwang, S. H. Jin, D. Y. Choi, S. D. Yoon and I. H. Lee, *Mater. Lett.*, 2014, **121**, 97–100.

21 H. L. Lv, G. B. Ji, X. H. Liang, H. Q. Zhang and Y. W. Du, *J. Mater. Chem. C*, 2015, **3**, 5056–5064.

22 M. Zhou, X. Zhang, J. M. Wei, S. L. Zhao, L. Wang and B. X. Feng, *J. Phys. Chem. C*, 2011, **115**, 1398–1402.

23 B. Zhao, G. Shao, B. B. Fan, W. Y. Zhao, Y. J. Xie and R. Zhang, *RSC Adv.*, 2014, **4**, 61219–61225.

24 S. He, G. S. Wang, C. Lu, X. Luo, B. Wen, L. Guo and M. S. Cao, *ChemPlusChem*, 2013, **78**, 250–258.

25 T. Y. Huang, M. He, Y. M. Zhou, S. W. Li, B. B. Ding, W. L. Pan, S. Huang and Y. Tong, *RSC Adv.*, 2016, **6**, 100392–100400.

26 X. Ding, Y. Huang, S. P. Li, N. Zhang and J. G. Wang, *Composites, Part A*, 2016, **90**, 424–432.

27 D. Z. Chen, H. Y. Quan, G. S. Wang and L. Guo, *ChemPlusChem*, 2013, **78**, 843–851.

28 X. H. Guan, P. Gu and G. S. Wang, *RSC Adv.*, 2014, **4**, 15579–15585.

29 H. L. Lv, Y. H. Guo, Y. Zhao, H. Q. Zhao, B. S. Zhang, G. B. Ji and Z. C. J. Xu, *Carbon*, 2016, **110**, 130–137.

30 M. Fu, Q. Z. Jiao, Y. Zhao and H. S. Li, *J. Mater. Chem. A*, 2014, **2**, 735–744.

31 H. L. Lv, H. Q. Zhang, G. B. Ji and Z. C. Xu, *ACS Appl. Mater. Interfaces*, 2016, **8**, 6529–6538.

32 M. Zhou, F. Lu, B. Chen, X. Y. Zhu, X. S. Shen, W. W. Xia, H. He and X. H. Zeng, *Mater. Lett.*, 2015, **159**, 498–501.

33 G. Wang, X. Peng, L. Yu, G. Wan, S. Lin and Y. Qin, *J. Mater. Chem. A*, 2015, **3**, 2734–2740.

34 Y. Liu, X. X. Liu, R. Liu, W. Wu and X. J. Wang, *RSC Adv.*, 2015, **5**, 8713–8720.

35 Y. P. Duan, Z. Liu, H. Jing, Y. H. Zhang and S. Q. Li, *J. Mater. Chem. A*, 2012, **22**, 18291–18299.

36 G. P. Wan, L. Yu, X. G. Peng, G. Z. Wang, X. Q. Huang, H. N. Zhao and Y. Qin, *RSC Adv.*, 2015, **5**, 77443–77448.

37 M. Zhou, F. Lu, T. Y. Lv, X. Yang, W. W. Xia, X. S. Shen, H. He and X. H. Zeng, *J. Phys. D: Appl. Phys.*, 2014, **48**, 215305–215311.

38 H. L. Lv, H. Q. Zhang, J. Zhao, G. B. Ji and Y. W. Du, *Nano Res.*, 2016, **6**, 1813–1822.